ISSN 1990-7931, Russian Journal of Physical Chemistry B, 2020, Vol. 14, No. 2, pp. 377–389. © Pleiades Publishing, Ltd., 2020.
Russian Text © The Author(s), 2020, published in Khimicheskaya Fizika, 2020, Vol. 39, No. 4, pp. 80–92.

CHEMICAL PHYSICS
OF ATMOSPHERIC PHENOMENA

Formation of Ionospheric Irregularities in the East Siberian Region during the Geomagnetic Storm of May 27–28, 2017

D. S. Kotova[a, b, *], I. E. Zakharenkova[a], M. V. Klimenko[a], V. B. Ovodenko[a], I. V. Tyutin[c, d], D. V. Chugunin[a, e], A. A. Chernyshov[a, e], K. G. Ratovsky[f], N. V. Chirik[a], M. V. Uspensky[g], V. V. Klimenko[a], R. A. Rakhmatulin[f], A. Yu. Pashin[f], A. V. Dmitriev[d, h], and A. V. Suvorova[d, h]

[a] *Pushkov Institute of Terrestrial Magnetism, Ionosphere, and Radio Wave Propagation, Kaliningrad Branch, Russian Academy of Sciences, Kaliningrad, 236010 Russia*
[b] *Department of Physics, University of Oslo, Oslo, 0371 Norway*
[c] *JSC Scientific and Research Institute for Long-Distance Radio Communication, Moscow, Russia*
[d] *Skobeltsyn Institute of Nuclear Physics, Moscow State University, Moscow, 119991 Russia*
[e] *Space Research Institute, Russian Academy of Sciences, Moscow, 117997 Russia*
[f] *Institute of Solar-Terrestrial Physics, Siberian Branch, Russian Academy of Sciences, Irkutsk, 664033 Russia*
[g] *Finnish Meteorological Institute, Helsinki, 00560 Finland*
[h] *National Central University, Taoyuan, 32001 Taiwan*
**e-mail: darshu@ya.ru*

Received February 20, 2019; revised May 7, 2019; accepted May 20, 2019

Abstract—Results of studying different-scale ionospheric irregularities on the basis of multi-instrumental data, obtained in the East Siberian region of Russia during the geomagnetic storm of May 27–28, 2017, are presented. Spatial inhomogeneities of electron density in the ionosphere were observed through data from ground-based receivers of signals of global navigational satellite systems and on the basis of direct measurements of electron density in low-orbit satellites. An intense radio aurora was seen in UHF radar data just after the initial phase of geomagnetic storm. At the same time, we recorded fluctuations of the total electron content from data of GPS receivers and the presence of E-layer irregularities by data of the ionosonde in Norilsk. The time of irregularity recording by different instruments is consistent with the spatiotemporal changes in field-aligned currents of the second zone, obtained from data of AMPERE low-orbit satellite system.

Keywords: ionospheric irregularities, radio aurora, Birkeland currents, auroral precipitation, high-latitude ionosphere

DOI: 10.1134/S1990793120020232

INTRODUCTION

The high-latitude ionosphere is a strongly structured medium, in which a large amount of irregularities at different scales, from a few meters to hundreds of kilometers, is formed [1]. The irregularities are structured by latitude according to the subdivision of high-latitude ionosphere into the subauroral and auroral ionospheres, polar cap and cusp/cleft zones. The high-latitude irregularities are mainly a result of the action of processes of magnetosphere–ionosphere interaction, associated with the auroral activity, in particular, with photochemical processes, with allowance for impact ionization by energetic magnetospheric particles and processes of plasma transfer and warming up due to electric fields and field-aligned currents. In [2], the mechanisms of action of different energetic particles on the atmosphere are discussed. In turn, the plasma irregularities and aeronomic effects in the atmosphere may have a considerable influence on the quality of the satellite and high frequency (HF) radio communication, the functioning of radiolocation stations (radars) and navigational satellite systems. Basic understanding of the formation of the different-scale plasma irregularities in the high-latitude ionosphere and about their impact on the radio communication are given in the monographs [3–7]. Issues of the influence of ionospheric irregularities in high latitudes on radar functioning have been considered separately [8–10].

The high-latitude ionosphere is one of the main regions of the localization of intense small-scale instabilities and irregularities in electron density [11–14], which may be related to the electric fields and intense precipitations of high-energy particles in this region. Additionally, kinetic processes on a small scale may have the appreciable influence on large-scale processes at high latitudes, which lead to the heating and formation of ion fluxes, as well as to the formation of

regions with the increased plasma density [15]. Precipitations of high-energy charged particles lead not only to the profile modification of the background electron density, but also to the situation that the ionospheric plasma becomes more irregular. As a result, the transionospheric radio signals of GPS/GLONASS navigational satellite systems undergo the stronger scintillations than the mid-latitude ionospheric scintillations during transfer through this irregular medium. This may lead to an ambiguity of operation of algorithms for correction of empiric ionosphere models by data of receivers of the global navigational satellite system (GNSS), which are located in the high-latitude region [16]. As demonstrated in [17], where a moderate substorm was studied, the simultaneous increase in the total electron content (TEC) and in phase scintillations obtained using GPS receiver, as well as the increased flux of thermal electrons, takes place, which was established by measurements of the DMSP low-orbit satellites.

In periods of geomagnetic storm, the largest number of faults in navigational measurements and, consequently, in the TEC determination takes place near the auroral oval [18]. The necessity of performing detailed studies of ionospheric influence on the propagation of navigational signals in high-latitude regions is shown in [19, 20]. The dynamics of the faults of the parameters of GPS navigational signals within the period from 2010 to 2014 was studied in [21] for stations located in the Arctic region. The probabilities of instrumental loss of phase and pseudo range, as well as short-term variations in the large rate of TEC change under different geomagnetic conditions, were analyzed. It is shown that the probabilities of the fault for TEC are much (100- to 200-fold) higher than instrumental error and grow considerably during geomagnetic storms and substorms. It is also necessary to note that due to the navigational signal scattering on small-scale irregularities of electron density (with a size of irregularity on the order of a size of the Fresnel first zone, amounting to 100–300 m), strong scintillations in the amplitude and phase of signals in the GPS receiver are observed [22, 23]. The relationship of the signal amplitude scintillation at the GPS operating frequency L1 to failures of the given signal reception was shown in [24]. UHF-range radars, functioning at high latitudes, also are subjected to the influence of ionospheric irregularities. A link between scintillations and a quality of radar measurements, namely the signal amplitude and phase, was shown in [25–27]. These characteristics are especially important for radars, since they determine a reliability of target detection.

To study the causes of the spatial structure formation and its connection with dynamics of ionospheric irregularities of different scales during the geomagnetic storm, we used a multi-instrumental approach in this work. As an example, we selected a period of moderate geomagnetic storm, May 27–28, 2017. The selection of this period was motivated by the availability of radar data, the coverage of which included the Norilsk region. The multi-instrumental approach was based on using satellite and ground-based data, which characterize both different-scale ionospheric irregularities and the magnetospheric influence on the ionosphere in the region under study. As a source of information for the multi-instrument study in the high-latitude East Siberian region within a period from May 27 to May 28, 2017, we used data of a ground-based GNSS receiver, UHF radar, Swarm and DMSP low-orbit satellites, stations of vertical ionospheric sounding, ground-based magnetometers, and magnetometers of the orbital satellite constellation of Active Magnetosphere and Planetary Electrodynamics Response Experiment (AMPERE). The use of this set of heterogeneous data makes it possible to estimate the presence of links in occurrence of different-scale ionospheric irregularities at different ionosphere altitudes: in the E- and F-regions of ionosphere, as well as in the external ionosphere.

1. DESCRIPTION OF THE SPACE WEATHER PHENOMENON UNDER STUDY

In this study, we considered the ionospheric response to the geomagnetic storm of May 27–28, 2017. Figure 1 shows parameters and indices, characterizing the helio-physical situation within a period from May 26 to May 29, 2017. These data were taken from the OMNI database. The moderate geomagnetic storm began on May 27, 2017, after 15:00 UT. The storm under consideration was characterized by rather a long phase of sudden commencement. The main storm phase fell on transition from May 27 to May 28 according to UT time and was characterized by a drop in the *Dst* index value down to –125 nT at 07:00 UT on May 28. The maximum value of *AE* index was observed in a period from 04:00 to 08:00 UT on May 28 and reached values of ~1500 nT. The recovery phase of geomagnetic storm began approximately at 10:00 UT on May 28, 2017, and continued up to 12:00 UT on May 29.

The geomagnetic storm under study originally was initiated by fast changes in solar wind speed and pressure. The next development of the storm arose after the overturn of the B_z component of the interplanetary magnetic field from northern to southern direction. As can be seen from Fig. 1, the behavior of the K_p index agrees well with the B_z-component behavior.

2. DATA USED

2.1. Detection of Different-Scale Ionospheric Irregularities

By the present time, measurements of time delays in propagation of radio signals of GPS/GLONASS navigational satellite systems are one of main sources of monitoring of the ionosphere state on the global

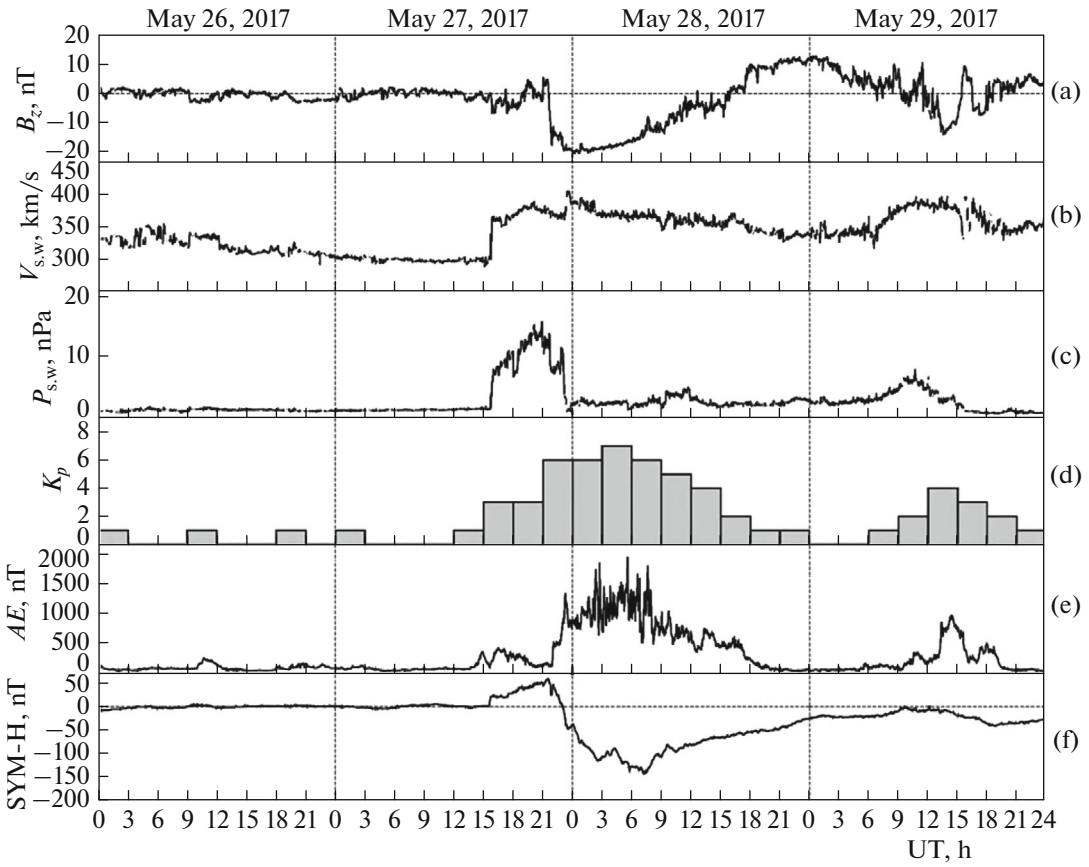

Fig. 1. Variations of the interplanetary magnetic field (IMF), solar wind parameters and geomagnetic indices for May 26–29, 2017 (from top to bottom): (a) B_z component of IMF, (b, c) speed and dynamic pressure of solar wind, (d) 3-h global index of geomagnetic activity K_p, (e) auroral electrojet index AE, and (f) index of ring current development SYM-H.

scale under quiet and disturbed conditions. In [23], two new metrics ROT and ROTI were introduced into use for ground-based GPS measurements. The ROT (rate of TEC) metric describes the rate of TEC change on the 1-min interval and is the indicator of the presence of the signal phase fluctuations. The metrics ROTI (rate of TEC index), is the standard deviation of ROT over a fixed time interval, characterizes the intensity of phase fluctuations and is used for detecting plasma irregularities and spatial gradients. Both indices are widely used in space weather services and in studies of the high-latitude and equatorial plasma irregularities in data from ground-based GPS receivers [19, 28, 29].

In this work, for studying the occurrence of ionospheric irregularities during geomagnetic disturbances, the analysis of GPS data from three ground-based stations was performed: NRIL (Norilsk, 69.3° N, 88.3° E), DIKS (Diksi, 73.5° N, 80.4° E), and NOVM (Novosibirsk, 55.0° N, 82.9° E). The geographic location of the stations is shown in Fig. 3. These stations provide GPS measurements with a time resolution of 30 s, which allows them to be used for detecting irregularities with spatial scales of the tens to the hundreds of kilometers. For this purpose, the variation in the ROT index variation was calculated for all visible GPS satellites (with an angle of elevation of more than 20°) over the station on the daily interval. This kind of measurements allows the ionosphere to be monitored within the radius of ~7°–10° with respect to the station position on the horizontal scale. We additionally used the direct measurements of electron density at the altitude of ~460 km by data of Swarm satellites and at the altitude of ~800 km by data of the DMSP F16 satellite.

To study irregularities in the lower ionosphere (E-region), we analyzed the radio echo, recorded by a powerful large-aperture radar of UHF range with the northern orientation of the coverage area, which was located near Krasnoyarsk (56° N, 93° E). This radar covers distances up to 2000 km in the azimuth sector of ~100° at the elevation angle of 3°. The period of radar measurements is 5 s. The minimum aspect angle for this radar is 3°, which determines its ability to observe radio aurora. We will analyze a range of altitudes from 80 to 150 km among all data of the radar. The radio echo at altitudes of ~90–130 km corresponds to: (1) radio aurora [9, 30] (inverse aspect scattering of radio waves on ionospheric magnetically-ori-

ented irregularities (MOI) with a longitudinal size equal to half-wavelength of radar signal, i.e., about 35 cm); (2) meteoric echo [31] (radio echo from ionized meteor trails, as well as from meteoric head).

To record ionospheric irregularities in the HF band, we used the data of the DPS-4 ionosonde, located in Norilsk. The ionosonde of vertical sounding operates with an interval of 15 min. The ionogram data were analyzed, which made it possible to reveal moments of arising of sporadic layer of E-, F-scattering and the total absorption of a radio signal (blackout) and to compare these moments with formation of irregularities detected by other aids.

2.2. Observations of Parameters of Magnetosphere–Ionosphere Interaction

To analyze the response of local variations of geomagnetic field to the geomagnetic storm, in this work, the data from the magnetometer in Norilsk (geomagnetic coordinates: 59.9° N, 166.7° E) were used. The maintenance and data processing of this magnetometer is performed at the Institute of Solar-Terrestrial Physics of Siberian Branch of Russian Academy of Sciences. In this study, we analyzed changes in the vertical component of geomagnetic field dZ in the form of a difference of this component values under quiet and disturbed conditions: $dZ = Z_s - Z_q$, where Z_s and Z_q are the vertical components of the magnetic field during the storm and for a quiet day, respectively. In this case, the data for May 26, 2017, were used as Z_q, while data for May 27 and 28 were chosen as Z_s. We note that the Z axis is directed toward the zenith.

To study the latitude–time variability of the system of Birkeland field-aligned currents in the period of the event under study, we used the data of magnetometers of the Iridium system, containing more than 70 low-orbit satellites (with an orbit altitude of 780 km). The AMPERE project [32] uses satellites with an orbit inclination of 86°, which are distributed uniformly between six equally located orbital planes. This makes it possible to obtain information on the radial current density, calculated in the corrected geomagnetic coordinate system. The AMPERE satellite constellation provides global observations of field-aligned currents of the first, second, and third zones over the northern and southern high-latitude regions within the latitude interval from 90° to 50°. Additionally, to determine the boundary of auroral precipitations and velocities of horizontal electromagnetic drifts at separate moments of time, we used data from DMSP satellites.

3. DISCUSSION OF RESULTS

3.1. Latitudinal Borders of Ionospheric Irregularities at Different Altitudes

Figure 2 presents the dependence of radio echo (radio aurora and meteor echo), recorded within an altitude range of 90–130 km in a time period from 23:20 to 23:30 UT on May 27, 2017. The coordinates measured by the radar (distance, azimuth, and elevation angle) were recalculated into geographic coordinates of reflection points and plotted on the map. As can be seen from Fig. 2, the equatorial border of the radio aurora is ~66.5°, while the pole border is ~68°. The latitudinal extension of radio aurora is explained by the geometry of its observation by the radar: the backscattering of radio waves from irregularities of the ionospheric E-layer occurs in the altitude range of 90–130 km. The longitudinal extension of radio aurora is determined by two factors: azimuthal scanning of radar in a range of ~100° and by a change in aspect angles from 3° to ~15° depending on azimuth. With an increase in the aspect angle, the energy of signal, scattered from MOI [30], decreases from 5 to 15 dB by a degree. This leads to a decrease in the signal/noise and, consequently, the probability of the radio aurora detection.

Figure 3 shows the geographic location of three GPS stations (the analysis of data of which is presented below) and a projection of the Swarm A satellite (orbit altitude is 465 km) flight over the region under study about 00:00 UT on May 28, 2017. On the right of Fig. 3, the comparison of variations of electron density along the flight of the Swarm A satellite on the storm day of May 28, 2017, and on the quiet day of May 26, 2017. In the quiet day, the ionospheric irregularities of weak intensity were observed, mainly, in the more polar direction of 75–80° N. On the disturbed day of May 28, 2018, the analogous flight of the satellite, corresponding to ~07:00 LT (0 UT), recorded the expansion of a zone of ionospheric irregularities up to 60° N. It should be noted that under disturbed conditions, by contrast with quiet ones, a main ionospheric trough (MIT) is revealed on this flight at the latitude of ~73° N. In this case, the geographic latitude of the MIT minimum is slightly further northward than the radio aurora border, shown in Fig. 2. This speaks to the fact that the MIT low-latitude wall forms partly due to the precipitations of auroral electrons, responsible for the irregularity formation at altitudes of the lower ionosphere, which lead to the radio aurora. A border of irregularities at altitudes of the Swarm A satellite flight approximately coincides with borders of radio aurora.

At satellites of DMSP series the cold plasma measurements also were conducted. Figure 4 shows the electron density measurements (panel a) and the ion drift velocities (panel b), obtained at the altitude of about 800 km onboard the DMSP F16 satellite which was flying across the region of reflection of radar radio signals. It should be noted that the oscillations, connected with the ionospheric irregularities above the F2 layer, are observed in relation to the behavior of electron density at the external ionosphere altitudes in both the Swarm A and DMSP F16 flights. By contrast to the equatorial border of radio reflections, the region of these irregularities began from ~61° N; therefore,

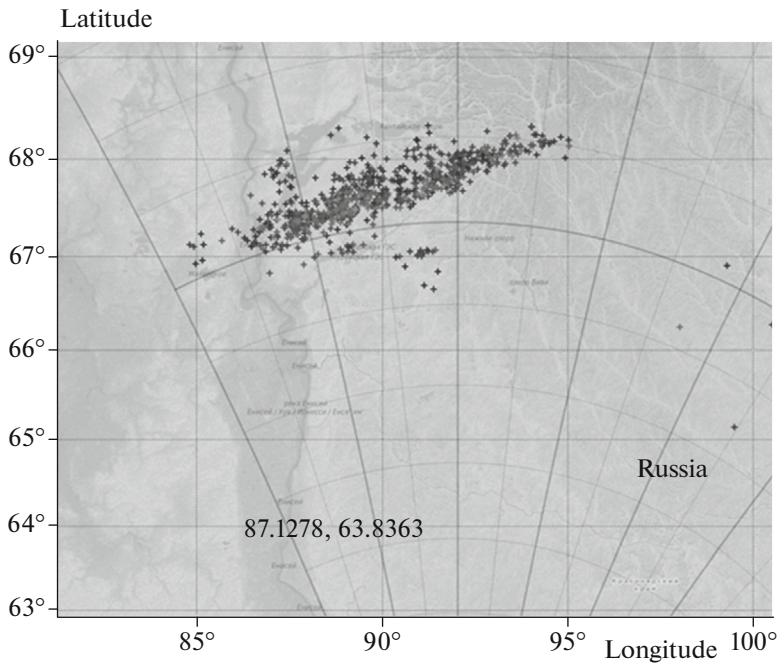

Fig. 2. Radio echo in the altitude range of 90–130 km in the latitude–longitude coordinates, recorded for the time interval from 23:20 to 23:30 UT on May 27, 2017, by UHF radar in the Krasnoyarsk area.

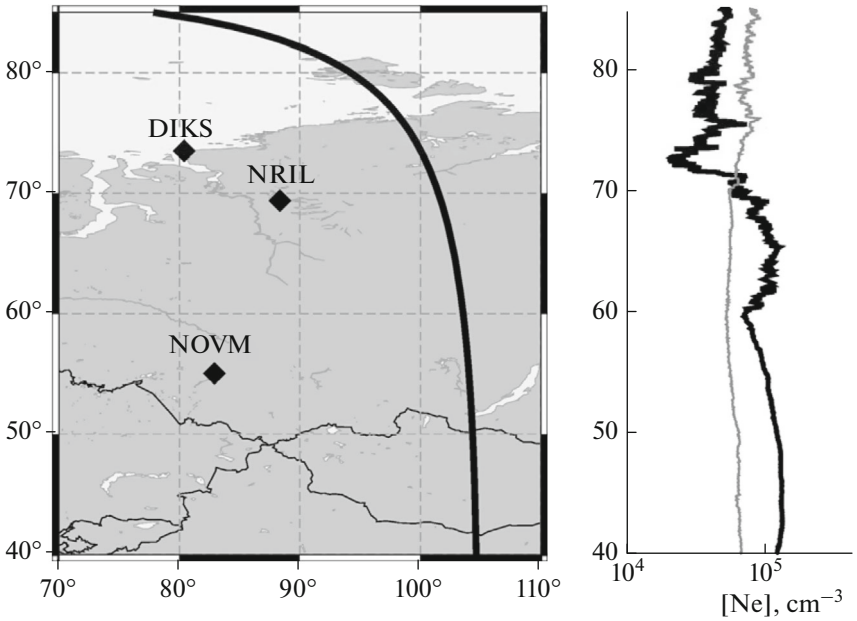

Fig. 3. (*Left panel*) Geographic map with the location of three GPS stations (NOVM, NRIL, and DIKS) and the flight trajectory projection of the Swarm A satellite (black thick line) for May 28, 2017, in the period 00:14–00:35 UT. (*Right panel*) Latitudinal profile of the electron density variation along the flight trajectory of Swarm A satellite on the storm day of May 28, 2017 (black thick line) and on the quiet day of May 26, 2017 (grey thin line).

the cause of their occurrence had no direct link with the radio aurora. Thus, the latitudinal extension of recorded irregularities differs from the irregularity extension at altitudes of the ionosphere E-region. A characteristic difference in the ion drift velocity can be seen further equatorward and poleward of the radio aurora border, especially in the velocity of horizontal drift. At the latitudes further northward, the strong

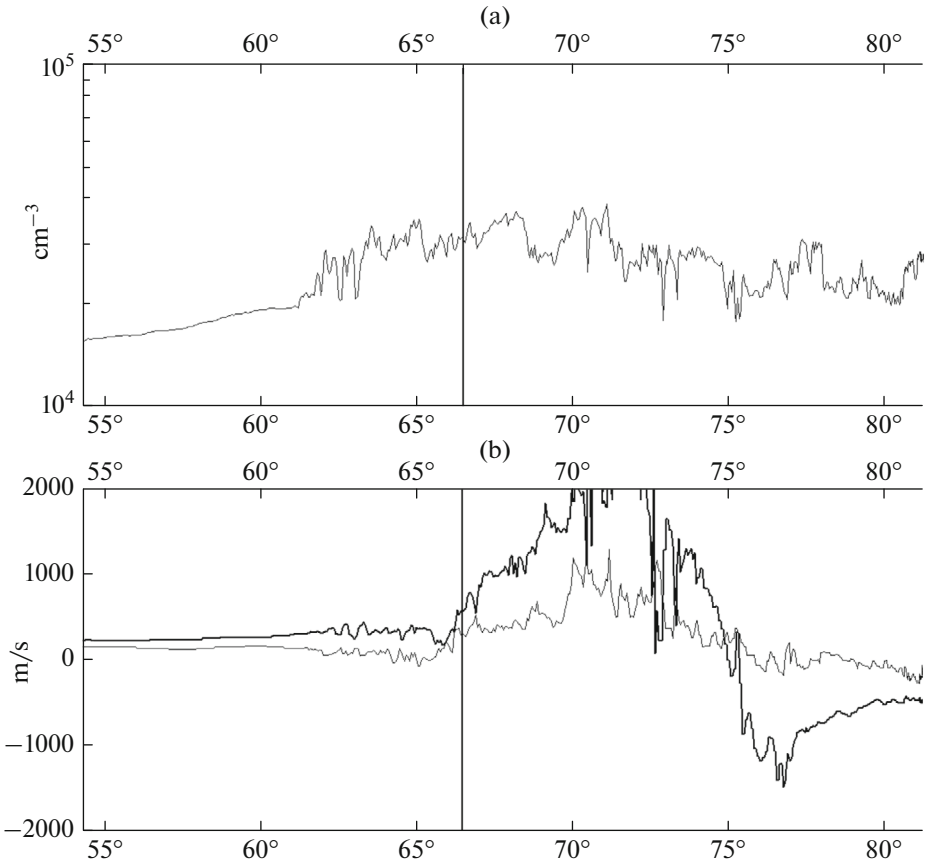

Fig. 4. Measurements of (a) electron density and (b) ion drift velocity, performed during the flight of the DMSP F16 satellite on May 27, 2017, within the time period from 23:13 to 23:23 UT. On the horizontal, the geographic latitude of the satellite position is laid off; on the vertical, (a) density and (b) velocity are plotted. The vertical line (~66.5° N) denotes a latitude of the equatorial border of the radio aurora. In Fig. 4b, the black thick line shows the horizontal drift, and the thin grey line indicates the vertical drift of ion velocity.

plasma convection prevails, which is driven by strong electric fields in the auroral zone.

At the spectrograms in Fig. 5, the DMSP F16 satellite measurements of differential fluxes of electrons and ions H^+ are presented. From comparison of latitudinal borders of the radio aurora (Fig. 2) with borders of auroral precipitations, as well as with measurements of electron density and ion drift velocity (Fig. 4), a link of these processes is evident. It can be seen from the measurements that main precipitations of energetic particles fall on the zone before the satellite crossing of the radio-reflection region. The radio aurora corresponds to the region of precipitations of particles with energy of 100–1000 eV near 66.5° N. The borders of the radio aurora are located slightly further poleward than the equatorial border of auroral precipitations. From this, it follows that the radio wave reflections occur in irregularities in the lower ionosphere, which are driven by structured precipitations in the region of upward current.

3.2. Development of Disturbances over Time

Figure 6 presents the dependence of radio echo of UHF radar in time–altitude coordinates within the azimuth sector of ~100°. Vertical lines separate three cases: (1) the time of quiet geomagnetic conditions in the auroral zone and the initial phase of geomagnetic storm, which resulted in the intense radio aurora (onset at ~22:33 UT on May 27); (2) the time interval of ~1.5 h (03:20–04:50 UT on May 28) when the radio aurora intensity abruptly decreased; and (3) the time interval with an evolution of radio aurora intensity from intense to weak during the recovery stage of geomagnetic storm. For the first case, the sharp rise in the radio echo intensity is observed within the altitude range from 100 to 130 km. The reflections in the time interval of 22:10–22:33 UT on May 27 correspond to the weak radio aurora and reflections from meteors. The intense radio aurora had a duration of ~13 h, up to 10:55 UT on May 28, 2017. As a whole, the time interval under study covers the complex and prolonged geomagnetic storm consisting of several substorm activations.

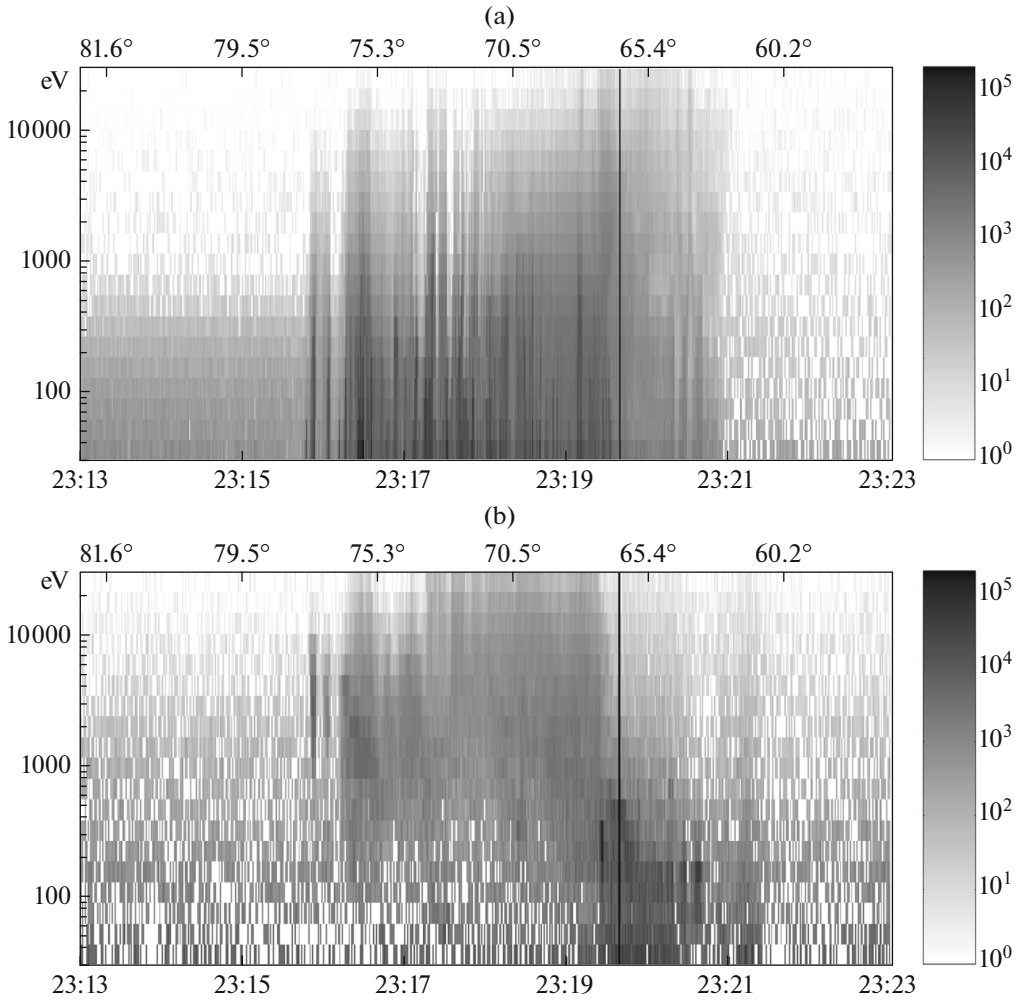

Fig. 5. Measurements of precipitations of (a) electrons and (b) ions, performed onboard the DMSP F16 satellite on May 27, 2017. The lower horizontal axis shows the UT time, on the upper horizontal axis, the geographic latitude of the satellite position at the given time moment. The vertical axis shows the energy of particles in eV. Black and white shading shows the intensity of the differential flux of high-energy particles (particle/(eV sr s cm^2)). The vertical black line shows the latitude of the equatorial border of the radio aurora.

The phenomenon of a drop in radio aurora intensity for the second case (see above) within a period of 03:25–04:55 UT on May 28, 2017, probably, is related to a decrease in the ionospheric electric field and to a change in the direction of ionospheric convection [33]. We do not have a continuous data set of direct measurements of ionospheric electric field in the region under study; however, below, an analysis of time distribution of the field-aligned current for the storm under study by AMPERE data is presented.

Figure 7 presents the ROT index variations for three ground-based GPS stations indicated on the map (see Fig. 3) and for all observed GPS satellites during the two days of May 27–28, 2017. The satellites were recorded within the radius of ~7°–10° with respect to the station position on the horizontal scale. It should be noted that under normal (undisturbed) conditions for the mid-latitude stations the ROT index typically varies about zero values, within the limits of ±1 TECU/min. In Fig. 7, this ROT variation looks like a horizontal line with very small fluctuations during the entire period of satellite observation (a few hours). As can be seen in Fig. 7, before the storm commencement on May 27, 2017, this ROT-index behavior is observed at all three stations. After the onset of disturbance, a significant enhancement of fluctuations in the ROT value, exceeding 3–5 TECU/min, was observed, which corresponded to intense ionospheric irregularities. The enhancement of phase fluctuations firstest (~16:00 UT on May 27) was fixed at the DIKS (higher-latitude) station. At the NRIL station, these fluctuations were recorded after ~1800–20:00 UT on May 27 and had a less pronounced nature. With the enhancement of auroral activity (AE > 1000 nT) after ~22:00 UT on May 27 at the DIKS and NRIL high-latitude stations, the significant amplification (ROT > ±5 TECU/min)

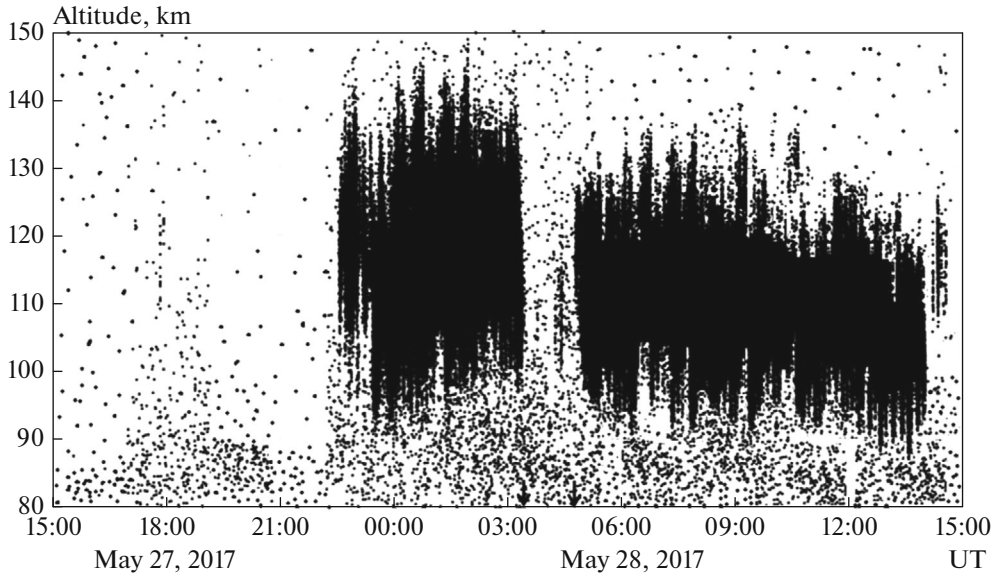

Fig. 6. Dependence of radio echo by the UHF radar data in altitude–time coordinates for May 27–28, 2017. Black dots show the radio echo, recorded at unique time moments.

of phase fluctuations of navigational signals is recorded for all visible satellites. With further development of the storm (~00:00–03:00 UT on May 28) over the NRIL station, more intense ionospheric irregularities are observed than for the higher-latitude DIKS station, which is associated with an expansion of the auroral irregularity oval and its displacement towards the lower latitudes. However, for the NOVM mid-latitude station, the variations in the ROT index appeared very quiet, both before and after the commencement of the storm. The latter testifies to the fact that the ionospheric irregularities of auroral origin did not reach the level of 55° N with the development of this storm.

Figure 8 shows examples of ionograms for the data of the station for the vertical sounding of the ionosphere in Norilsk. From the analysis of the ionogram sequence for May 27 and 28, we can note that (1) distinct trails from the E and F2 layers (while at daytime also from the F1 layer) were seen on May 27 up to 16:00 UT; (2) from 16:00 to 17:15 UT the E layer was developing; (3) from 17:45 to 20:00 UT, ionograms over Norilsk were very variable, with total absorption being replaced by the strong F-scattering (Fig. 8a); (4) from 20:15 to 21:00 UT, the ionograms indicated the development of an inhomogeneous sporadic E-layer over Norilsk (Fig. 8b); (5) from 21:30 to 01:30 UT on May 28, information on ionograms was almost absent (at this time, only at separate time moments could a part of the E-layer trail be seen on ionograms); (6) from 01:30 to 03:00 UT on May 28, distinct trails from the sporadic E-layer appeared (Fig. 8c); (7) from 0330 to 12:00 UT on May 28, information on ionograms was almost absent (at this time, only at separate time moments, a part of the E-layer trail could be seen on ionograms). The absence of information on ionograms in the end of May 27 and for half of May 28 could have been caused by a total signal absorption at altitudes of the lower ionosphere and by the significant density reduction in the F-region over Norilsk. They may both be related to the fact that Norilsk at that time was in the region of auroral and more intense precipitations of energetic particles. That is, due to electron-density reduction in the F-region, even in the absence of the recording of ionospheric irregularities in radar data from 03:30 to 04:50 UT on May 28, the ionograms do not indicate the presence of trails from ionospheric layers.

Next, to study the causes of the occurrence of ionospheric irregularities in the region under consideration, we used satellite and ground-based data on magnetic field variations and compared them for quiet and disturbed conditions. We analyzed changes in the vertical component dZ of the geomagnetic field in Norilsk (Fig. 9). At the station, negative variations dZ were observed from ~16:00 UT on May 27, corresponding to magnetospheric compression (Fig. 9a). This compression led to an increase in the component Z, which was directed downward in the northern hemisphere (negative component Z). Consequently, the increase in the negative value of the component Z resulted in an increase in the negative dZ. From 22:00 to 24:00 UT, strong variations were observed in dZ, which were created by the high-latitude western electrojet. From 22:13 to 23:12 UT, a significant growth of dZ on the order of a few hundred of nT was observed on the magnetometer. From 23:13 to 24:00 UT on May 27, strong negative variations of dZ with values of up to 300 nT were observed. These changes in the magnetic field were driven by the displacement of the western

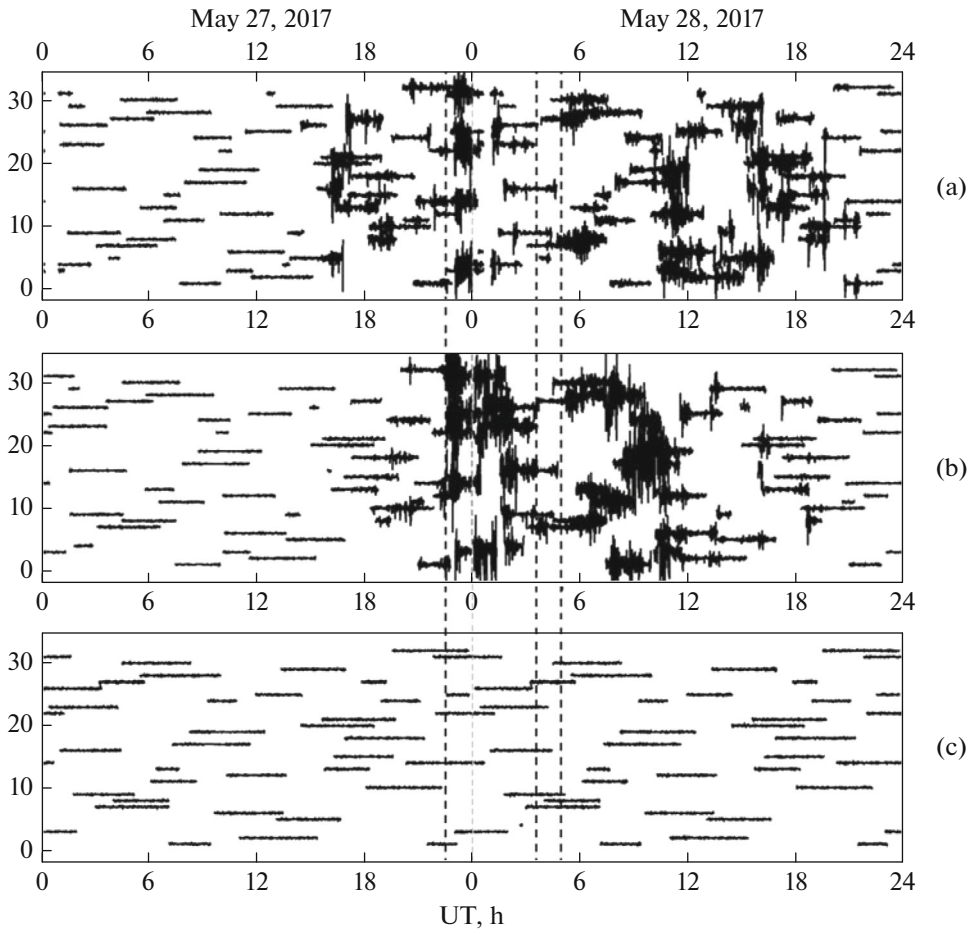

Fig. 7. ROT-index variations for the ground-based GPS stations ((a) DIKS), (b) NRIL, and (c) NOVM) and all GPS satellites observable during two days: May 27–28, 2017. On each panel, the vertical axis denotes a number of the observable GPS satellite: from 1 to 32; vertical black dashed lines correspond to the time moments: 22:34, 03:23, and 04:54 UT.

electrojet from high latitudes through Norilsk toward the equator. From 00:00 to ~02:30 UT on May 28 (Fig. 9b), significant variations in the positive value of dZ with an amplitude of ~500 nT were observed. These changes were associated with the strong auroral electrojet and intense auroral activity over Norilsk. The other time interval of strong variations of negative values of dZ with the amplitude of up to 600 nT was observed in the period from ~08:30 to ~11:00 UT on May 28. This interval corresponded to the displacement of the western electrojet toward the equator and to the intense auroral activity southward of Norilsk.

Let us compare the time of irregularity recording at different instruments with the spatiotemporal changes in field-aligned currents of the second zone, obtained from data of the AMPERE low-orbit satellite system on the geomagnetic longitude of Norilsk. Data of the radial current density, presented in Fig. 10, are calculated in the corrected geomagnetic coordinates.

Under quiet geomagnetic conditions, a border of location of field-aligned currents of the first and second zones is near the geomagnetic latitude of 65°–75°. In Fig. 10, it can be seen that both the enhancement of currents and the displacement (by ~10° in latitude) of the region of flow of field-aligned currents toward the equator are observed during the storm. During the event under study, the displacement of a border of the second zone currents up to the Norilsk latitude occurs. The time interval of this displacement of the region of field-aligned currents agrees well with the time of observing the radio aurora on the radar (Fig. 6) from 22:30 UT on May 27 to 14:00 UT on May 28. The appearance of an intense radio echo at 22:35 UT on May 27 corresponds to maximum density values of the effluent and influent currents of the second and first zones, respectively (to 2 $\mu A/m^2$ in modulus). The regions of intense precipitations of high-energy electrons (auroras) coincide spatially with regions of the field-aligned current effluent from the ionosphere [34]. The comparison of Figs. 7 and 10 indicates the link of significant changes (ROT > ±5 TECU/min) of phase fluctuations of navigational signals over Norilsk and Diksi with the enhancement and displacement of field-aligned currents of the second zone. Moreover,

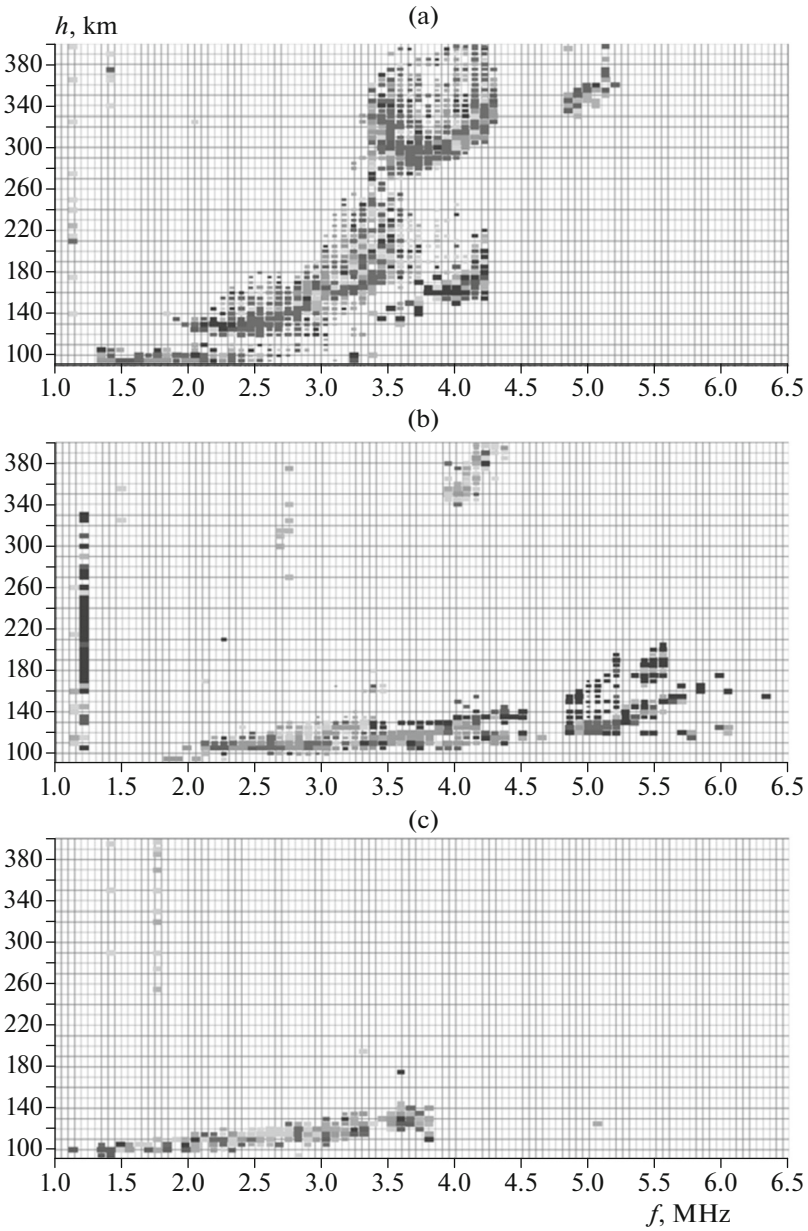

Fig. 8. Ionograms of vertical sounding over Norilsk for (a) 19:00 UT on May 27; (b) 20:45 UT on May 27; and (c) 02:45 UT on May 28.

on Diksi, the phase fluctuations begin to be observed from 16:00–17:00 UT on May 27. From Fig. 10 it can be seen that at the geomagnetic latitude of Diksi (~65°) at the indicated time of May 27, the rather significant upward currents of the second zone (-0.5 μA/m^2) are observed. In the period from 03:20 to 04:50 UT on May 28 by data of the radar (Fig. 6) and the GNSS receiver in Norilsk (Fig. 7), a decrease in the intensity of both radio aurora and ROT variations are observed. This weakening of the inhomogeneous structure of ionosphere, probably, is connected with processes of sign change of field-aligned currents of the second and first zones and with the relevant attenuation of these currents. It can be noted that after the sign change of the second zone currents, the average altitude of the radio aurora reflections varied: it reduced approximately by 10 km. The presence of intense phase fluctuations from 05:00 to 11:00 UT on May 28 over Norilsk is associated with the location of the border of field-aligned currents of the second zone near the GPS-signal receiver. In the period under study, the ionograms on the ionosonde in Norilsk are absent due to the strong absorption of the emitted signal in the environment. If a comparison with results of electron density observation at Swarm A is performed, then it should be noted that the density drop between 73°–75°

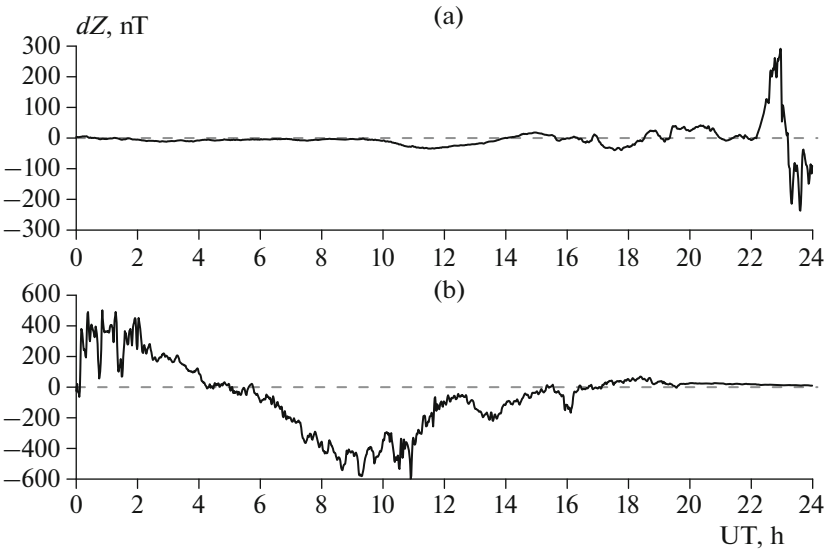

Fig. 9. Deviations of vertical magnetic component *dZ* during the geomagnetic storm on (a) May 27 and (b) May 28, 2017, obtained by data of the magnetometer in Norilsk.

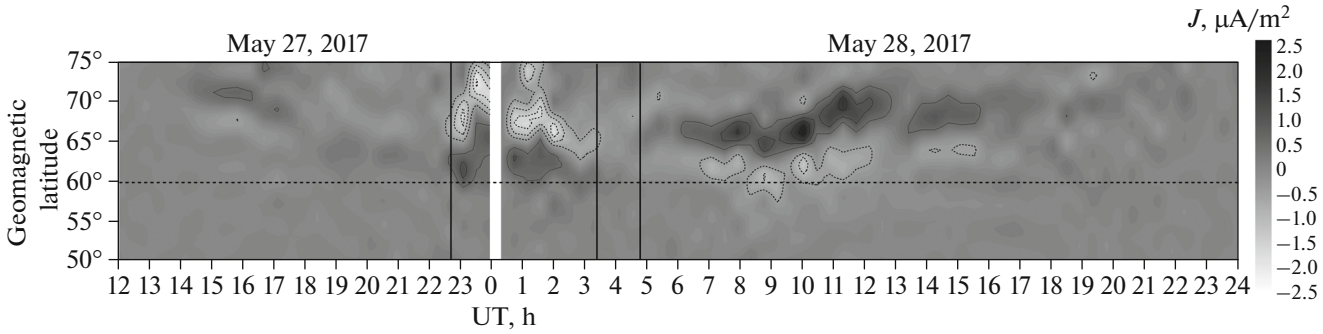

Fig. 10. Map of time distribution of radial current density, obtained at the fixed geomagnetic longitude of Norilsk within an interval of geomagnetic latitudes from 50° to 75°. The dashed horizontal line marks the position of Norilsk on the geomagnetic latitude of 59.9°. The currents, effluent from the ionosphere, are shown in black color (positive values) and by solid isolines, while the currents influent into the ionosphere are shown in white color (negative values) and by dotted isolines. The time moments of appearance and disappearance of radar reflections, according to Fig. 6, correspond to vertical lines.

of geographic latitude (63°–65° of geomagnetic latitude) at the indicated time moment (00:14–00:35 UT) can be related to the satellite flight through the region of field-aligned currents of the second zone.

CONCLUSIONS

The high-latitude ionosphere is a strongly structured medium due to the presence of a large amount of irregularities at different scales, arising from complex processes of the interaction between the magnetosphere and ionosphere. In periods of geomagnetic disturbances, the formation of the strongest irregularities and nonstationarity of the plasma occurs. This work presents a multi-instrument review of spatiotemporal variations of different-scale ionospheric irregularities in the East Siberian region during the geomagnetic storm of May 27–28, 2017.

The main results of the study can be formulated as follows. The large-scale irregularities of a size of ~10–100 km and the TEC variations associated with them were recorded by GPS receivers in Norilsk and Diksi, but the receiver in Novosibirsk did not record the ROT appreciable changes during the storm under study. The small-scale irregularities in the E layer with the longitudinal size on the order of 35 cm were recorded by the UHF radar in the Norilsk area. The ionosonde in Norilsk also fixed the formation of intense irregularities in the E layer and the significant time interval with a total absorption of HF radio waves. The latter indicated that Norilsk was inside the auroral oval in the time period under study.

We revealed the coincidence between the appearance of the intense radio aurora and the growth in the ROT index at the high-latitude and auroral stations during the geomagnetic storm. The time of occurrence of ionospheric irregularities and their recording are agreed with the spatiotemporal variations of field-aligned currents of the second zone. In the regions of formation of ionospheric irregularities, strong electric fields and the increased ion drifts are observed. The period of reduction of the intensity of the radio aurora (03:20–04:50 UT on May 28, 2017) agrees with the time of sign change of field-aligned currents.

ACKNOWLEDGMENTS

The authors acknowledge the European Space Agency for provision of data of the Swarm mission (http://earth.esa.int/swarm), the National Geophysical Data Center (NGDC NOAA) for submission of the DMSP data (satdat.ngdc.noaa.gov/dmsp/data), and also the International GNSS Service (IGS) for the GPS data of ground stations (ftp://cddis.gsfc.nasa.gov/pub/gps/). The authors also are grateful to the Institute of Applied Geophysics and personally V.V. Alpatov for furnished data of GPS/GLONASS receivers. The space weather data were made available by NASA/GSFC's Space Physics Data Facility's OMNIWeb service (http://omniweb.gsfc.nasa.gov/). The authors thank G. Coxon for provision of the AMPERE data on field-aligned currents.

FUNDING

This work was supported by the Russian Science Foundation (project no. 17-77-20009). The analysis and processing of data of the ionosonde and magnetometer in Norilsk were supported by the Russian Foundation for Basic Research within the scientific project no. MOST-107-2923-M-008-001-MY3/18-55-52006MNT_a (K.G. Ratovskii, A.V. Dmitriev, A.V. Suvorova, and R.A. Rakhmatulin).

REFERENCES

1. M. J. Keskinen and S. L. Ossakow, Radio Sci. **18**, 1077 (1983). https://doi.org/10.1029/RS018i006p01077
2. E. V. Rozanov, Russ. J. Phys. Chem. B **12**, 786 (2018). https://doi.org/10.1134/S0207401X18070154
3. G. A. Zherebtsov, Yu. G. Mizun, and V. S. Mingalev, *Physical Processes in the Polar Ionosphere* (Nauka, Moscow, 1988) [in Russian].
4. B. E. Bryunelli and A. A. Namgaladze, *Physics of the Ionosphere* (Nauka, Moscow, 1988) [in Russian].
5. B. Hultqvist, M. Oieroset, G. Paschmann, et al., Space Sci. Ser. ISSI **6** (7) (1999).
6. R. D. Hunsucker and J. K. Hargreaves, *The High-Latitude Ionosphere and its Effects on Radio Propagation* (Cambridge Univ. Press, Cambridge, 2002).
7. R. W. Schunk and A. F. Nagy, *Ionospheres: Physics, Plasma Physics, and Chemistry* (Cambridge Univ. Press, Cambridge, 2009), p. 268.
8. B. A. Bagaryatskii, Usp. Fiz. Nauk **63**, 197 (1961).
9. R. L. Leadabrand, J. C. Schlobohm, and M. J. Baron, J. Geophys. Res. **70**, 4235 (1965). https://doi.org/10.1029/JZ070i017p04235
10. R. L. Leadabrand, A. G. Larson, and J. C. Hodges, J. Geophys. Res. **72**, 3877 (1967).
11. J. Aarons, J. Geophys. Res. A **102**, 17219 (1997). https://doi.org/10.1029/97JA01118
12. A. A. Chernyshov, A. A. Il'yasov, M. M. Mogilevskii, I. V. Golovchanskaya, and B. V. Kozelov, Plasma Phys. Rep. **41**, 254 (2015).
13. A. A. Ilyasov, A. A. Chernyshov, M. M. Mogilevsky, et al., Phys. Plasmas **22**, 032906 (2015). https://doi.org/10.1063/1.4916125
14. A. A. Ilyasov, A. A. Chernyshov, M. M. Mogilevsky, I. V. Golovchanskaya, and B. V. Kozelov, Russ. J. Phys. Chem. B **12**, 527 (2018).
15. D. V. Chugunin, M. V. Klimenko, A. A. Chernyshov, V. V. Klimenko, A. A. Il'yasov, and R. Yu. Luk'yanova, Geomagn. Aeron. **58**, 50 (2018). https://doi.org/10.7868/S0016794018010054
16. D. S. Kotova, V. B. Ovodenko, Yu. V. Yasyukevich, M. V. Klimenko, A. A. Mylnikova, A. E. Kozlovsky, and A. A. Gusakov, Russ. J. Phys. Chem. B **12**, 776 (2018). https://doi.org/10.1134/S0207401X18070129
17. S. Basu, E. MacKenzie, S. Basu, et al., Radio Sci. **18**, 1151 (1983).
18. E. Astafyeva, Yu. Yasyukevich, A. Maksikov, et al., Space Weather **12**, 508 (2014). https://doi.org/10.1002/2014SW001072
19. J. Aarons and B. Lin, J. Atmos. Sol.-Terr. Phys. **61**, 309 (1999). https://doi.org/10.1016/S1364-6826(98)00131-X
20. S. C. Mushini, P. T. Jayachandran, R. B. Langley, et al., GPS Solutions **16**, 363 (2012). https://doi.org/10.1007/s10291-011-0238-4
21. V. I. Zakharov, Yu. V. Yasyukevich, and M. A. Titova, Cosmic Res. **51**, 20 (2013). https://doi.org/10.7868/S002342061601143
22. K. C. Yeh and C. H. Liu, IEEE Proc. **70**, 324 (1982).
23. X. Pi, A. J. Mannucci, U. J. Lindqwister, et al., Geophys. Rev. Lett. **24**, 2283 (1997).
24. B. M. Ledvina, J. J. Makela, and P. M. Kintner, Geophys. Rev. Lett. **29** (14) (2002). https://doi.org/10.1029/2002GL014770
25. J. T. Reinking, L. D. Knepp, and A. M. Hausman, Radio Sci. **36**, 1157 (2001). https://doi.org/10.1029/1999RS002413
26. D. L. Knepp, Radio Sci. **50**, 1 (2011). https://doi.org/10.1109/URSIGASS.2011.6050974
27. D. L. Knepp, Radio Sci. **50**, 968 (2015). https://doi.org/10.1002/2015RS005740

28. C. Watson, P. T. Jayachandran, E. Spanswick, et al., J. Geophys. Res. **116**, A00I90 (2011). https://doi.org/10.1029/2010JA015732

29. I. Cherniak, A. Krankowski, and I. Zakharenkova, GPS Solutions **22**, 69 (2018). https://doi.org/10.1007/s10291-018-0730-1

30. M. V. Uspenskii, G. V. Starkov, and L. S. Evlasnin, *Auroras and Scattering of Radio Waves* (Nauka, Leningrad, 1987), p. 237 [in Russian].

31. S. Close, S. M. Hunt, F. M. McKeen, et al., Radio Sci. **37** (1) (2002). https://doi.org/10.1029/2000RS002602

32. S. E. Milan, J. A. Carter, H. Korth, et al., J. Geophys. Res. Space Phys. **120**, 415 (2015). https://doi.org/10.1002/2015JA021680

33. M. V. Uspensky, P. Janhunen, A. V. Koustov, et al., Ann. Geophys. **29**, 1081 (2011). https://doi.org/10.5194/angeo-29-1081-2011

34. C. L. Waters, B. J. Anderson, and K. Liou, Geophys. Rev. Lett. **28**, 2165 (2001). https://doi.org/10.1029/2000GL012725

Translated by M. Samokhina